

# Reconstructing plant root area and water uptake profiles

by

Kiona Ogle<sup>1</sup>, Robert L. Wolpert<sup>2,3</sup>, James F. Reynolds<sup>1,3</sup>

Duke University, <sup>1</sup>Department of Biology, <sup>2</sup>Institute of Statistics and Decision Sciences, and <sup>3</sup>Nicholas School of the Environment and Earth Sciences, Durham, North Carolina 27708 USA

## Abstract

A major challenge in plant ecology is quantifying how roots interact with the soil to obtain water and nutrients. Stable isotope analysis of hydrogen and oxygen bound in plant and soil water is one of the best and least destructive methods for elucidating plant-soil interactions. Plant roots obtain water from various depths in the soil and the isotopic signature of plant stem water reflects the soil water sources. However, current methods for inferring plant water sources based on stable isotopes ("simple linear mixing models") are limited. First, their formulation restricts the number of water sources to a maximum of three (e.g., surface, intermediate, deep soil water); estimation of additional sources leads to an identifiability problem. Second, simple linear mixing models do not appropriately reflect uncertainty, and most importantly, they cannot be employed to elucidate behavior of the root system itself such as root activity for water uptake. This study introduces the RAPID (Root Area Profile and Isotope Deconvolution) algorithm, a novel and powerful approach for reconstructing plant water uptake and root area profiles. The RAPID algorithm overcomes the nonidentifiability problem by incorporating a biophysical model for root water uptake into a Bayesian framework such that the biophysics and prior distributions place biologically realistic constraints on the profiles. Posterior distributions for the proportions of active root area and water acquired from each soil layer are obtained via Markov chain Monte Carlo. Finally, RAPID is applied to data collected for a desert shrub and employed to examine sampling implications.

**Key words:** inverse problem; water uptake; MCMC;  $\delta D$ ;  $\delta^{18}O$ ; creosotebush; *Larrea tridentata*; soil water; soil texture; plant water relations; deconvolution; identifiability; Bayesian; RAPID

## Introduction

The unraveling of belowground processes, especially root-soil interactions whereby plants acquire water and nutrients from the soil matrix, remains one of the greatest challenges in plant ecology. Two key questions are: Where do active roots occur within the soil profile? and from where in this soil profile are roots obtaining water? Advances in the analysis of stable isotopes of hydrogen and oxygen bound in plant and soil waters offers one of the most powerful and least destructive tools for addressing these questions (Dawson & Ehleringer, 1998, Ehleringer & Dawson, 1992). Both the evaporative process, as well as rain events of varying isotopic compositions, result in soil water content and isotope profiles that vary with soil depth (Allison & Hughes, 1983, Ehleringer & Dawson, 1992). Heavy water comprised of deuterium (D) and/or  $^{18}\text{O}$  evaporates slower than light water, leaving water near the soil surface enriched in D and  $^{18}\text{O}$  (Barnes & Allison, 1988).

The uptake of water by roots at different soil depths occurs without fractionation (Thorburn *et al.*, 1993, Walker & Richardson, 1991). Thus, the isotopic signature of water in the plant stem is the average of the soil water isotopic values weighted by the proportion of water acquired from each soil layer. Simple linear mixing (hereafter, SLM) models have been developed to estimate these weights based on the isotopic composition of the plant and source water. SLM models have been derived to determine the relative contribution of two (Thorburn & Walker, 1993, White *et al.*, 1985) or three (Brunel *et al.*, 1995, Cramer *et al.*, 1999) water sources, to infer the importance of seasonal rainfall (Ehleringer *et al.*, 1991, Schwinning *et al.*, 2002), groundwater (Ewe *et al.*, 1999, Snyder & Williams, 2000), fog or cloud water (Feild & Dawson, 1998), and different soil layers (Plamboeck *et al.*, 1999, Retzlaff *et al.*, 2001) to plant water uptake and its implications for plant adaptive strategies and community interactions.

Although useful, there are significant limitations to SLM models. They are restricted to a maximum of three water sources, and can not be employed to estimate additional sources because multiple solutions render the proportions of water acquired from each source unidentifiable. When used to estimate contributions of two or three sources, they may yield inconsistent proportions (Thorburn & Ehleringer, 1995) that are occasionally negative (e.g., Brunel *et al.*, 1995, Snyder & Williams, 2000) or greater than one (e.g., Ewe *et al.*, 1999) and

do not adequately account for uncertainty in the estimated proportions (Brunel *et al.*, 1995, Phillips & Gregg, 2001a, Phillips & Gregg, 2001b). Lastly, SLM models are inappropriate for making inferences about the root system itself, such as active root area, which is essential for elucidating plant-soil interactions.

To overcome the shortcomings of SLM models, we present a new and comprehensive algorithm for reconstructing active root area and water uptake profiles: RAPID (Root Area Profile and Isotope Deconvolution). The RAPID algorithm employs stable isotopes to estimate profiles of root water uptake and, most importantly, it enables us to reconstruct root area dynamics and to explicitly account for uncertainty in these estimates. Our approach reduces the identifiability problem by integrating a biophysical model for root water uptake into a Bayesian inverse modeling framework (e.g., Neath & Samaniego, 1997). The biophysical model and prior distributions place realistic biological constraints on root area profiles. In this paper, we describe the RAPID algorithm, demonstrate its veracity and power with synthetic data, apply it to field data collected for a desert shrub, and address its implications for sampling design.

## The Inverse Problem

SLM models provide estimates of the proportion ( $p_i$ ) of water obtained by a plant from, for example, two adjacent soil depths ( $i = 1$  vs.  $2$ ). If either the relative abundance of D ( $\delta D$ ) or  $^{18}\text{O}$  ( $\delta^{18}\text{O}$ ) is measured then a set of two equations is solved for  $p_1$  and  $p_2$ . If both  $\delta D$  and  $\delta^{18}\text{O}$  are measured, contributions from three sources can be similarly estimated, provided the isotopes are not highly correlated (Brunel *et al.*, 1995), by solving a set of three equations:

$$\begin{aligned}\delta D_{stem} &= p_1 \cdot \delta D_1 + p_2 \cdot \delta D_2 + p_3 \cdot \delta D_3 \\ \delta^{18}O_{stem} &= p_1 \cdot \delta^{18}O_1 + p_2 \cdot \delta^{18}O_2 + p_3 \cdot \delta^{18}O_3 \\ p_1 + p_2 + p_3 &= 1\end{aligned}\tag{1}$$

where  $\delta X_{stem}$ ,  $\delta X_1$ ,  $\delta X_2$ , and  $\delta X_3$  ( $X = \text{D}$  or  $^{18}\text{O}$ ) are the stem and the three source water signatures.

We take a different approach and first note that in reality the isotope signature of the stem water is the integral of the soil water isotope profile,  $\delta X_{soil}(v)$ , convolved with the root water uptake profile,  $q(v)/\int q(v)dv$ :

$$\delta X_{stem} = \int \delta X_{soil}(v) \cdot \frac{q(v)}{\int q(v)dv} dv \quad [2]$$

where  $q(v)$  is the flux of water from the soil to the root. Eqn [2] assumes that measurements are made as continuous functions of soil depth ( $v$ ) whereas, in practice, individual soil layers are discretely sampled, yielding:

$$\delta X_{stem} \cong \sum_{i=1}^N \delta X_{soil,i} \cdot \frac{q_i}{\sum_{j=1}^N q_j} \quad [3]$$

Theoretically, one measures  $\delta X_{stem}$  and  $\delta X_{soil,i}$  for  $i = 1, \dots, N$  soil layers to estimate  $q_i/\sum q_i$ . If  $N = 2$  or  $3$  and  $q_i/\sum q_i$  is set to  $p_i$ , then [3] is equivalent to [1]. Our goal though is to reconstruct an important determinant of  $q_i/\sum q_i$  — root area for water uptake,  $RA_i$  — in addition to  $q_i/\sum q_i$ . This is an inverse problem because a unique solution may not exist and  $q_i$  and thus  $\delta X_{stem}$  are highly nonlinear functions of  $RA_i$  (e.g., [4]). To minimize the non-uniqueness problem (for  $N > 3$ ), we developed the RAPID (Root Area Profile and Isotope Deconvolution) algorithm, which couples a biophysical model for root water uptake, stable isotope measurements, and a Bayesian inverse modeling approach.

## The RAPID Algorithm

**The Biophysical Model for Root Water Uptake.** While there are many models of varying complexity for root water uptake ( $q_i$ ,  $\text{mg}\cdot\text{sec}^{-1}$ ), we employ Campbell's (1991) formulation because it is relatively simple, yet captures key elements of root-soil interactions:

$$q_i = \frac{2 \cdot RA_i}{r_r \cdot (1-n)} \left( \ln \left( \frac{r_r \cdot RA_i}{2 \cdot l_i} \right) \right)^{-1} \cdot (k_{bs,i} \cdot \Psi_{bs,i} - k_r \cdot \Psi_r) \quad [4]$$

where  $r_r$  is mean root radius (m);  $n$  is a constant that varies with soil texture;  $k_{bs,i}$  and  $k_r$  are the hydraulic conductivities ( $\text{mg}\cdot\text{sec}\cdot\text{m}^{-3}$ ) of the bulk soil and at the root surface;  $\Psi_{bs,i}$  and  $\Psi_r$  are the water potentials (J/kg) of the bulk soil and at the root surface; and  $l_i$  is the height (m)

**Table 1.** Parameters and variables in the biophysical model for root water uptake [4].

Parameter	Description	Units	Value/equation*
$q_i$	Flux of water from the soil to the root in soil layer $i$	$\text{mg}\cdot\text{sec}^{-1}$	unknown
$RA_{tot}$	Total active root area	$\text{m}^2$	1.0
$RA_i$	Active root area in layer $i$	$\text{m}^2$	[5]
$f_{r,i}$	Fraction of active root area in soil layer $i$	–	unknown
$r_r$	Mean root radius	m	0.0001
$l_i$	Height of soil layer $i$	m	varies with $i$
$\theta_i$	Soil water content in layer $i$	g/g	measured
$\theta_s$	Saturated soil water content	g/g	0.252
$b$	Soil texture parameter <sup>†</sup>	–	2.1
$n$	Soil texture parameter	–	$2+3/b$
$k_s$	Saturated soil hydraulic conductivity	$\text{mg}\cdot\text{sec}\cdot\text{m}^{-3}$	1.7
$k_{bs,i}$	Hydraulic conductivity of bulk soil in layer $i$	$\text{mg}\cdot\text{sec}\cdot\text{m}^{-3}$	$k_s \left( \frac{\theta_i}{\theta_s} \right)^{2b+3}$
$k_r$	Hydraulic conductivity at the root surface	$\text{mg}\cdot\text{sec}\cdot\text{m}^{-3}$	$k_s \left( \frac{\Psi_e}{\Psi_r} \right)^{2+3/b}$
$\Psi_e$	Air entry potential	J/kg	–0.9
$\Psi_{bs,i}$	Water potential of bulk soil in layer $i$	J/kg	$\Psi_e \left( \frac{\theta_i}{\theta_s} \right)^{-b}$
$\Psi_r$	Water potential at the root surface	J/kg	measured

\* Equations for  $k_{bs,i}$ ,  $\Psi_{bs,i}$ ,  $k_r$ , and  $\Psi_r$  and values for  $b$ ,  $n$ ,  $k_s$ , and  $\Psi_e$  were obtained from Campbell and Norman [Campbell, 1998 #2]. We used Keith Saxton's "Soil Water Characteristics" v. 6.1.25 software (<http://www.bsye.wsu.edu/saxton/>) to estimate  $\theta_s$ .

<sup>†</sup> For synthetic data (see Appendix B), we assumed that all soils were sandy-loam, which is the soil type of a near-by site [Reynolds, 1999 #13]; we choose  $n$  to reflect this soil type. Assuming a fixed  $n$  is not problematic because we used it both in generating synthetic stem isotope data and in the RAPID algorithm for reconstructing the true root area and water uptake profiles. When we employed the RAPID algorithm to reconstruct *Larrea's* root area profile we used observed soil texture data, which varies across days and depths, in determining  $\theta_s$ ,  $b$ ,  $n$ ,  $k_s$ , and  $\Psi_e$  for each soil sample.

of soil layer  $i$ . We assume that  $k_r$  and  $\Psi_r$  do not vary with depth since they are properties of the bulk root system. We also assume that  $RA_i = 2 \cdot L_i \cdot l_i \cdot \pi \cdot r_r$  where  $L_i$  is the root length density (cm root  $\text{cm}^{-3}$  soil) and  $\pi = 3.14159$ . Table 1 provides a detailed description of the parameters and variables in [4]. We decompose active root area into:

$$RA_i = RA_{tot} \cdot f_{r,i} \quad [5]$$

where  $RA_{tot}$  is total active root area,  $RA_{tot} = \sum RA_i$ , and  $f_{r,i}$  is the fraction of active root area in soil layer  $i$ . The purpose of this study is to develop a method for estimating  $f_{r,i}$ .

**Likelihood, Priors and Posterior.** We assume that stem isotope data ( $\delta \dot{X}$ ) follow a bivariate normal distribution with known covariance matrix  $C_{D,O}$ . For  $t = 1, \dots, T$  days and  $m = 1, \dots, M$  stem observations per day, the likelihood of the observed data is proportional to:

$$\exp \left\{ -\frac{1}{2} \sum_{t=1}^T \sum_{m=1}^M \left[ \begin{pmatrix} \delta \dot{D}_{stem,t,m} - \delta D_{stem,t} \\ \delta^{18} \dot{O}_{stem,t,m} - \delta^{18} O_{stem,t} \end{pmatrix}' \cdot C_{D,O}^{-1} \cdot \begin{pmatrix} \delta \dot{D}_{stem,t,m} - \delta D_{stem,t} \\ \delta^{18} \dot{O}_{stem,t,m} - \delta^{18} O_{stem,t} \end{pmatrix} \right] \right\} \quad [6]$$

$\delta D_{stem,t}$  and  $\delta^{18} O_{stem,t}$  are given by [3], [4], [5] and corresponding day-specific measurements of soil water content ( $\theta_i$ ) and  $\Psi_r$  (Table 1). Optimization of [6] may result in multiple solutions for  $f_{r,i}$  (some of which are more biologically realistic than others), thus we incorporate prior knowledge about  $f_{r,i}$  and determine the posterior distribution of  $f_{r,i}$  that reflects the plant and soil data, given constraints imposed by the priors.

While there are many ways to represent the continuous root area profile,  $f_r(v)$ , we opted for a mixture of gamma densities:

$$f_r(v | \alpha_1, \alpha_2, \mu_1, \mu_2) \equiv \omega \cdot \mathbf{Ga}(\alpha_1, \mu_1) + (1 - \omega) \cdot \mathbf{Ga}(\alpha_2, \mu_2) \quad [7]$$

with shape parameters  $\alpha_1$  and  $\alpha_2$ , means  $\mu_1$  and  $\mu_2$ , and mixture weight  $\omega$ . Eqn [7] is fairly simple yet it captures a range of distributions, including unimodal and bimodal ones, both of which commonly describe root biomass distributions of plant species (e.g., Schenk & Jackson, 2002). Because  $\alpha_1$ ,  $\alpha_2$ ,  $\mu_1$  and  $\mu_2$  are positive, we choose a multivariate normal prior for  $\ln(\alpha_1)$ ,  $\ln(\alpha_2)$ ,  $\ln(\mu_1)$ ,  $\ln(\mu_2)$  and  $\text{logit}(\omega)$  with covariance matrix  $B$ :

$$\left( \ln(\alpha_1) \quad \ln(\alpha_2) \quad \ln(\mu_1) \quad \ln(\mu_2) \quad \text{logit}(\omega) \right)' \sim \text{No} \left( \begin{pmatrix} a_1 & a_2 & m_1 & m_2 & w \end{pmatrix}', B \right) \quad [8]$$

Parameter values in [8] were chosen to reflect current knowledge about the root distribution of the target plant of interest (see Appendix A). The  $f_{r,i}$  values are obtained by integrating  $f_r(v)$  (as given in [7]) over the appropriate depths.

**Metropolis–Hastings Markov Chain Monte Carlo Routine.** The joint posterior distribution of  $\phi = (\alpha_1, \alpha_2, \mu_1, \mu_2, \omega)$  is proportional to the likelihood [6] times the prior [8]. Because  $\phi$  enters into the likelihood in a highly nonlinear manner, through its relationship to root area, an analytical solution for the joint posterior and the marginal posteriors for  $f_{r,i}$  are unattainable. Thus, we employ a Metropolis-Hasting (Chib & Greenberg, 1995, Hastings, 1970, Metropolis *et al.*, 1953) Markov chain Monte Carlo (MCMC) algorithm to generate

samples from the posterior distributions (Robert & Casella, 1999). The MCMC procedure is as follows:

1. Generate starting values  $\phi^{(0)}$ .
  - 1.1. Do steps 2.2–2.7 to calculate the posterior probability density of  $\phi^{(0)}$ ,  $P(\phi^{(0)} | \text{Data})$ .
2. For  $j = 1$  to  $J$ :
  - 2.1. Generate proposal values  $\phi^*$  from a transition density  $Q(\phi^* | \phi^{(j-1)})$ .
  - 2.2. For each soil layer  $i$ , calculate  $f_{r,i}$  given  $\phi^*$  in 2.1 and [7].
  - 2.3. For each soil layer  $i$ , calculate  $q_i$  given  $f_{r,i}$  in 2.2, [4], and [5].
  - 2.4. Calculate the mean "proposed" stem isotope signatures given  $q_i$  in 2.3., observed soil isotope data, and [3].
  - 2.5. Calculate the likelihood,  $L(\text{Data} | \phi^*)$ , of the observed stem isotope signatures given the proposed mean values in 2.4. and [6].
  - 2.6. Calculate the prior probability density of  $\phi^*$  based on [8],  $P(\phi^*)$
  - 2.7. Calculate the posterior probability density of the proposed values given the observed stem data as:
 
$$P(\phi^* | \text{Data}) \propto L(\text{Data} | \phi^*) \cdot P(\phi^*)$$
  - 2.8. Calculate the acceptance ratio:
 
$$\lambda = \frac{P(\phi^* | \text{Data}) \cdot Q(\phi^{(j-1)} | \phi^*)}{P(\phi^{(j-1)} | \text{Data}) \cdot Q(\phi^* | \phi^{(j-1)})}$$
  - 2.9. Generate a uniform random number  $u \sim U[0,1]$ .
  - 2.10. If  $u < \lambda$  accept proposed values and set  $\phi^{(j)} = \phi^*$ ; otherwise set  $\phi^{(j)} = \phi^{(j-1)}$
  - 2.11. If  $j < J$  then return to 2.1, otherwise stop.

We specified  $Q(\cdot | \cdot)$  as a Gaussian random walk for  $\ln(\alpha_1)$ ,  $\ln(\alpha_2)$ ,  $\ln(\mu_1)$ ,  $\ln(\mu_2)$  and  $\text{logit}(\omega)$  (see Appendix C for details on  $Q(\cdot | \cdot)$  and selecting  $\phi^{(0)}$  in step 1). We ran multiple (5–10) chains to facilitate monitoring of convergence to the "true" posterior distribution (Cowles & Carlin, 1996, Gelman, 1996). The  $f_{r,i}$  values associated with each  $\phi^{(j)}$  are stored after each iteration, providing a sample from their joint (and marginal) posterior distribution.

## Applying the RAPID algorithm

We conducted a rigorous test of the RAPID algorithm using synthetic data generated from a variety of “known” root area profiles with large differences in their general shape. Results are provided in the Appendix B and four of the root area scenarios are given in Table 2.

**Field Study.** Field data were collected during summer 1998 for the evergreen desert shrub *Larrea tridentata* (creosotebush), a dominant species of the North American warm and hot deserts (Solbrig, 1977). The study was conducted at the Jornada Long-Term Ecological Research site in the Chihuahuan desert in southern New Mexico, USA. Reynolds et al. (1999) give complete details of the soil and vegetation at the general study site. Average annual precipitation at the Jornada Basin is 230 mm, the majority (65%) of which falls in the summer (July–October) as localized thunderstorms, and 25% falls in the winter (November–March) as rain and snow associated with frontal storms (Conley *et al.*, 1992).

Samples were collected on five days: 7/25, 7/26, 7/29, 7/31, and 8/2/98. A total of 17.2 mm of rain fell between 7/22 and 7/24, thus soils were sampled immediately after a relatively large rain event and during the subsequent dry-down period. On each day five woody stem samples were collected from a single shrub, with the same shrub being sampled on days 7/25 and 8/2. Predawn water potentials of small terminal plant shoots were measured with a Scholander-type pressure bomb to estimate root water potential,  $\Psi_r$  (McCully, 1999). Three evenly spaced soil cores were collected from beneath the canopy of the corresponding shrub. Thus, 15 (5 days  $\times$  3 cores/day) total soil cores were extracted, two of which were sampled to a depth of 45 cm, four to 60 cm and nine to 75 cm. Soil cores were divided into depth categories (layers) of 0–2, 2–5, 5–10, 10–20, 20–30, 30–45, 45–60, and 60–75 cm, with finer resolution near the surface to capture steep gradients in soil water content (Cable, 1980, Schlesinger *et al.*, 1987) and isotopic composition (Barnes & Allison, 1988, Brunel *et al.*, 1995). Within a core, each layer was homogenized and subsamples was obtained for measurements of soil water content ( $\theta_i$ ) and stable isotope composition.

Water was extracted from the stem and soil samples and analyzed for natural abundance of D and  $^{18}\text{O}$  at the Center for Stable Isotope Biogeochemistry at the University of California, Berkeley (see Appendix D for further details on field and laboratory methods).

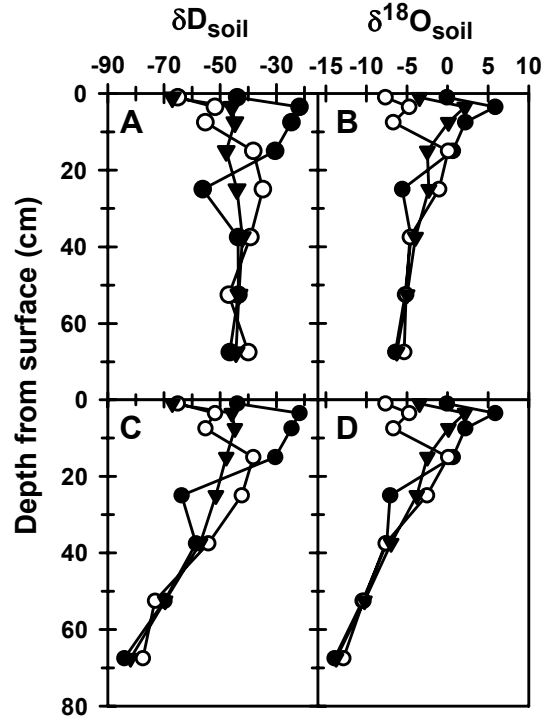


**Figure 1.** Examples of soil isotope profiles for three different soil cores collected on 8/2/98. A.) Measured  $\delta D_{\text{soil}}$ ; B) measured  $\delta^{18}O_{\text{soil}}$ ; C.)  $\delta D_{\text{soil}}$  profile transformed to increase the isotopic gradient for depths beyond 20 cm; D.) transformed  $\delta^{18}O_{\text{soil}}$  profile. Soil cores from the other four study days exhibit similar measured and transformed profiles.

Observed isotope and soil data were then supplied to the RAPID algorithm and 10 independent, parallel MCMC chains were simulated, each of length  $J = 10,000$ .

**Sampling Implications.** We evaluated the sensitivity of posterior estimates to alternative sampling strategies based on synthetic data sets for which the active root area and water uptake profiles were known. First we examined the effect of (soil) sampling resolution. We created a soil data set that reflected the common approach of sampling three layers. Soil samples were pooled into 0–10, 10–30, and 30–75 cm depth categories and soil water content in each *megalayer* was obtained by taking a weighted average of the measured  $\theta_i$  for the *sublayers*. For example, because we assumed a specific soil texture (see Table 1) and bulk density ( $\text{g soil cm}^{-3}$  soil) to generate the synthetic data, the water content of the 10–30 cm soil layer is given by  $\theta_{10-30} = (l_{10-20} \cdot \theta_{10-20} + l_{20-30} \cdot \theta_{20-30}) / 20$  where  $l_{10-20} = l_{20-30} = 10$  cm. Similarly, the stable isotope signature of the 10–30 cm layer is calculated as  $\delta X_{10-30} = 20 \cdot (\delta X_{10-20} \cdot l_{10-20} \cdot \theta_{10-20} + \delta X_{20-30} \cdot l_{20-30} \cdot \theta_{20-30}) / \theta_{10-30}$ . Before calculating the 3-layer soil data,

we simulated stem isotope samples based on the original, 8-layer soil data for root area Scenarios 2.1, 5.1, 5.2, and 5.3 (Table 2).

Second, we investigated the importance of the timing of sample collection, especially the sensitivity of the posterior estimates to soil water content. We compared the effect of sampling after rains with sampling during a dry period, during which soils near the surface contain little or no plant available water. We kept the initial sampling resolution (8 layers), but set all 15 soil water content profiles equal to the average soil water content profile of the first set of cores because they were collected immediately after a series of rains. We then simulated stem isotope samples based on the new, *rain*, soil samples and the four root area scenarios (Table 2).

Third, we examined how vertical variation in soil  $\delta\text{D}$  and  $\delta^{18}\text{O}$  affects the predicted active root area profile. Soil water isotopic signatures showed greater heterogeneity near the surface, but for depths beyond 20 cm, they converge to similar values and exhibit little variation (Fig. 1A, B). We transformed the soil isotopic data to yield a more pronounced gradient for depths exceeding 20 cm (Fig. 1C, D) and generated stem isotope data based on these transformed profiles for the root area scenarios in Table 2. For each of the three sampling schemes we input the simulated stem data and transformed soil data into the RAPID algorithm and ran 4 MCMC chains each of length  $J = 5,000$ .

## Results and Discussion

**Root Area Profiles for *Larrea tridentata*.** The reconstructed active root area profile for *Larrea* is shown in Fig. 2A. We are confident that this profile accurately depicts *Larrea*'s root system at the time and location of the field study because the 95% posterior credible intervals (CrI) (i.e., the 2.5<sup>th</sup> and the 97.5<sup>th</sup> quantiles of the MCMC posterior samples) for the fraction of root area in each soil layer are remarkably narrow. Although at first glance the profile appears unimodal, it actually has a small, but statistically significant fraction of root area in the top 2 cm (1.56%, 95% CrI = [1.15, 2.03]) (Fig. 2). Most (~96%) of the active root area is found between 20–45 cm. How does the reconstructed profile compare to previous studies? This is a difficult comparison because the RAPID algorithm gives active root area, but field studies typically measure physical attributes of the root system such as root

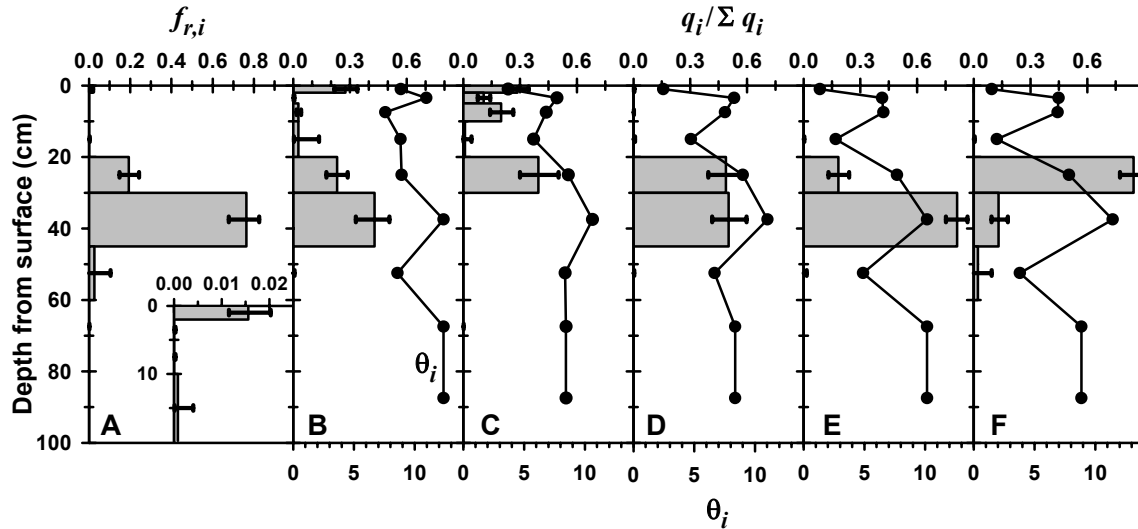


**Figure 2.** Posterior estimates of *Larrea*'s active root area distribution ( $f_{r,i}$ ) and water uptake ( $q_i/\sum q_i$ ) profiles. A.) Mean fraction of active roots in each soil layer; B.) mean fraction of water acquired from each soil layer on day 7/25/98, 1 day after moderate rainfall; C) water uptake fractions on day 7/26/98, 2 days after rainfall; D) water uptake fractions on day 7/29/98, 5 days after rainfall; E) water uptake fractions on day 7/31/98, 7 days after rainfall; F) water uptake fractions on day 8/2/98, 9 days after rainfall. Fractions depicted in the last layer represent cumulative fractions for depths beyond 75 cm. Mean soil water content of each layer ( $\theta_i$ ) is shown for reference.

biomass, which often does not reflect root function (Plamboeck *et al.*, 1999, Pregitzer *et al.*, 2002).

We found five studies that report (physical) root distributions for *Larrea* (Briones *et al.*, 1996, Freckman & Virginia, 1989, Kemp *et al.*, 1997, Moñtana *et al.*, 1995, Moorhead *et al.*, 1989). Two measured a large component (25–45%) of roots in the top 10 cm (Moñtana *et al.*, 1995, Moorhead *et al.*, 1989), and three suggest that there is substantial root mass (40–50%) between 20 and 50 cm (Briones *et al.*, 1996, Kemp *et al.*, 1997, Moorhead *et al.*, 1989). At least three (Briones *et al.*, 1996, Kemp *et al.*, 1997, Moorhead *et al.*, 1989) yield potentially bimodal distributions, but in two of the cases (Kemp *et al.*, 1997, Moorhead *et al.*, 1989) the soil sampling resolution was too coarse to clearly suggest bimodality. Moreover, Freckman (1989) collected soil samples in a *Larrea*-dominated site in the Jornada Basin to a depth of 400 cm and found that at least 80% of the roots occur in the top 100 cm. The other four studies suggest that nearly all of *Larrea*'s roots occur within the top 70–80 cm. Thus, it is likely that the maximum sampling depth of 75 cm did not limit our ability to reconstruct *Larrea*'s root profile.

What are the implications of the reconstructed active root area profile for *Larrea's* water uptake dynamics? The small fraction of active root area in the surface layers also appears to be biologically significant. While these roots normally contribute little to plant water uptake because water availability in shallow surface layers is typically very low (Sala *et al.*, 1992), their role may be to efficiently acquire water immediately after a rain event (e.g., Briones *et al.*, 1998). For example, nearly 30 to 40% of the water taken-up during the first and second days following the 17 mm rainfall came from the top 10 cm (Fig. 2B, C). This water source is likely to be very important to *Larrea's* growth and carbon balance because photosynthesis is often greatest following rains, when soil water content is relatively high (Reynolds *et al.*, 1999). Additionally, essential nutrients are concentrated in the topsoil (Jobbágy & Jackson, 2001) and a spike of root area near the surface may allow *Larrea* to capitalize on improved nutrient availability following rain (BassiriRad *et al.*, 1999). On the other hand, as the surface soils dried, the middle layers became the dominant water source and no water was acquired from the topsoil (Fig. 2C–F). The large fraction of active roots in the 20–45 cm range may serve to provide a stable water source that is essential for everyday function (Hacke *et al.*, 2000).

**Sampling Implications.** *Soil Sampling Resolution.* Posterior distributions of the root area fractions,  $f_{r,i}$ , were very sensitive to sampling resolution. Reducing the resolution from 8- to 3-layers dramatically increased both the uncertainty about the  $f_{r,i}$  values and the bias in their posterior means by an order of magnitude relative to the 8-layer sampling scheme (see MSE,  $MSE_{\text{mean}}$ ; Table 2). Even though the CrIs based on 3-layers were wider than those for 8-layers, they contained the true fractions less often (Table 2). In some cases, the widths of the 3-layer CrIs were equal to or close to the maximum value of one, which is completely uninformative. Importantly, the general shapes of the reconstructed profiles based on 3-layers differed greatly from the true shapes (Fig. 3B).

Thus, dividing the soil cores into many layers (e.g., 8+) is imperative for reconstructing root area and water uptake profiles with low bias and high confidence because it can capture fine-scale, depth-dependent variation in soil water content and isotopic composition. We suggest that the optimal sampling strategy is one that takes thin soil layers in regions where soil water and isotopic signatures are expected to exhibit high variability (e.g., near the surface). Preferably, a preliminary core should be obtained that is divided into



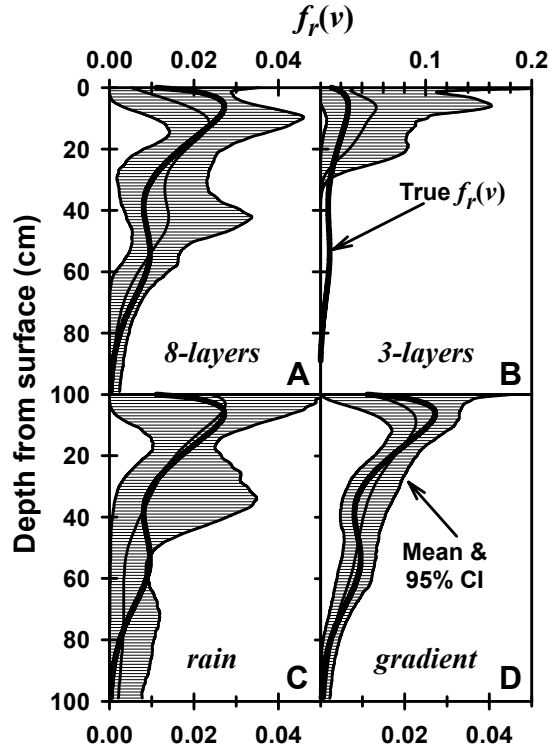


**Figure 3.** Posterior estimates of the continuous active root area profile for root area Scenario 5.5. The Posterior mean and 2.5<sup>th</sup> and 97.5<sup>th</sup> quantiles are overlaid with the true profile. Profiles are for the following sampling schemes: A.) actual soil data based on eight layers; B.) soil data pooled into three layers; C.) sampling after a rain, surface soils relatively wet; D.) soil isotope gradient increased (e.g.,). Notice that the x-axis scale differs for B.

scheme in 3 of the 4 root area scenarios (Table 2). But, the improvement is not enough (see Fig. 3C) to warrant restricting sample collection to days immediately following rainfall. However, we expect that sampling a day or two after irrigating with water spiked with D and <sup>18</sup>O concentrations that differ greatly from the ambient soil will improve the estimates because of the dual benefits of sampling moist soil and creating pronounced soil  $\delta$ D and  $\delta^{18}$ O gradients.

*Soil Isotopic Gradient.* Of the soil sampling protocols examined, the soil isotope gradient had the greatest impact on the posterior root area fractions. Increasing the  $\delta$ D and  $\delta^{18}$ O gradient for depths beyond 20 cm (Fig. 1) greatly reduced the MSE and MSE<sub>mean</sub> values and resulted in narrower CrI widths for each  $f_{r,i}$  (Table 2). The smaller CrIs were also able to capture the true fractions more often than any of the other sampling schemes. Furthermore,

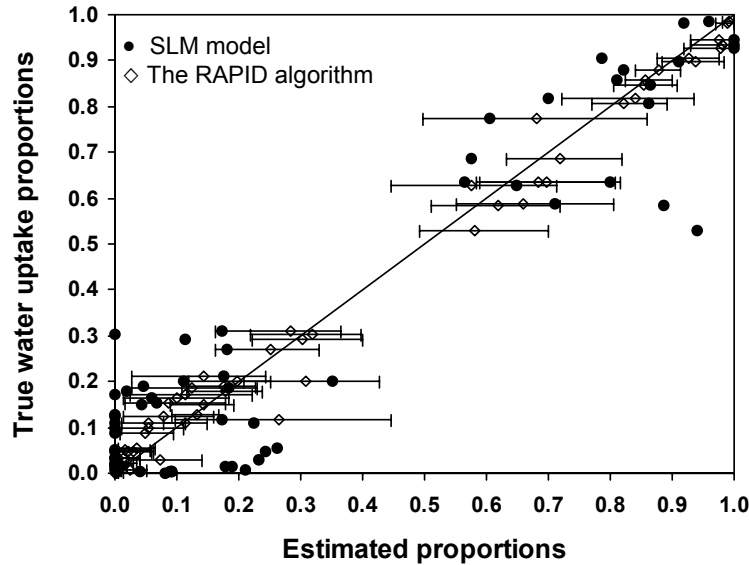


**Figure 4.** Comparison of estimated water uptake proportions from a 3-source simple linear mixing (SLM) model vs. the RAPID algorithm. Each point is the proportion of water acquired from 1 of 3 soil layers (0–10, 10–30, and 30–75 cm) and for one of 4 root area scenarios (Scenarios 2.1, 5.1, 5.2, and 5.3; Table 2). Filled circles are the SLM model proportions. Open triangles are the posterior means from the RAPID algorithm and the whiskers represent the 95% posterior CrI.

the reconstructed continuous root area profiles did exceptionally well at matching the shapes of the true profiles (Fig. 3D).

In practice, accuracy of the reconstructed root area profile will be enhanced for experiments that use isotope tracers to alter soil isotope gradients (e.g., Plamboeck *et al.*, 1999, Walker & Richardson, 1991) or for systems that exhibit high natural variability in soil isotope signatures. Natural gradients are expected to be intensified in areas that receive precipitation with a wide range of isotopic signatures (Ehleringer & Dawson, 1992), and Dansgaard (Dansgaard, 1964) provides examples of such locations. However, even in the absence of a strong profile, as in this study, the RAPID algorithm is able to successfully reconstruct a variety of root area profiles (also see Appendix B) and estimated *Larrea's* profile with high confidence.

**Simple Linear Mixing Models Revisited.** We now return to SLM models and compare their predictions with those generated by the RAPID algorithm. We fit a SLM model [1] to the 3-layer soil data and stem isotope data generated for root area Scenarios 2.1, 5.1, 5.2, and 5.3. We conducted a linear regression to obtain estimates for the proportion of water acquired from the three soil layers and constrained the proportions to lie between zero and

one. We also ran the RAPID algorithm with the original 8-layer soil isotope and water content data to obtain the fractions of water acquired from the eight layers and summed fractions from appropriate layers to obtain the uptake fractions for each of the three *megalayers*.

We evaluated true vs. predicted uptake fractions and estimates of the SLM model fall along the 1:1 line, but are more scattered ( $R^2 = 0.87$ ) and the regression slope and intercept diverge more from one and zero compared to the estimates of the RAPID algorithm (Fig. 4). The proportions yielded by the RAPID algorithm are clearly better as they lie closer to the 1:1 line and are tightly correlated with the true values ( $R^2 = 0.99$ ). Moreover, when the SLM model proportions were not constrained to lie between zero and one, 22% of the estimates fell outside of this range, deviating more from the true values ( $R^2 = 0.79$ ). However, the constrained SLM model results are in general agreement with the true fractions.

We also compared the water uptake fractions predicted by the two methods for *Larrea* based on the observed stem isotope and soil data. The two methods yielded strikingly different estimates that were uncorrelated with each other ( $R^2 = 0.03$ ). When not constrained, the SLM model resulted in uptake fractions greater than one or less than zero in four out of 15 cases. Additionally, the mean water uptake fractions given by the SLM model suggested that 21%, 4%, and 75% of the water was acquired from the 0–10, 10–30, and 30–75 cm soil layers, respectively. Conversely, the RAPID algorithm estimated that 18%, 44%, and 38% of the water was derived from the top, middle and deep layers over the course of the study period. Given these discrepancies and our thorough analysis of the RAPID algorithm, we are substantially more confident in its predictions.

## **Conclusions and Future Directions**

Utilizing stable isotopes of hydrogen and oxygen bound in plant and soil water, we present a novel algorithm for reconstructing active root area and water uptake profiles. The RAPID algorithm can be modified to increase its flexibility in two main ways. First, we employed Campbell's (1991) water flux model, but it could be exchanged for a more detailed model that captures, for example, steep gradients in soil hydraulic conductivity near the root surface (Sperry *et al.*, 1998) or depth-dependent variations in soil or root hydraulic properties (Wan

*et al.*, 1994) or root morphology (Vandenbeldt, 1991). We expect that these alterations will have little effect on root area and water uptake distributions (see sensitivity analysis in Appendix E), but may impact estimates of total root area (Caldwell & Richards, 1986) – a parameter that the algorithm thus far has not been employed to estimate. If isotope and soil data are accompanied by data on whole plant transpiration and within plant water potential gradients, this approach has the potential to estimate total root area ( $RA_{tot}$  [5]).

Second, the RAPID algorithm could be modified to incorporate different root area distributions or a hierarchical extension. In this study, we used a mixture of gammas to represent the root area profile [7]. Other continuous distributions, or mixtures thereof, could be employed, including an exponential, Weibull, beta, or a dirichlet for explicitly describing the proportions of root area in a finite number of soil layers. Root growth and biomass profiles can exhibit temporal or seasonal fluctuations (Fernandez & Caldwell, 1975, Reynolds *et al.*, 1999); vary across species, life-forms, or functional types (Fernandez & Caldwell, 1975, Midwood *et al.*, 1998); differ across sites (Weaver, 1982); and adjust due to dynamic allocation patterns (Huang & Fu, 2000). Thus, it is likely that active root area exhibits similar behavior, hence a hierarchical specification that allows the parameters of the profile (e.g.,  $\alpha_1$ ,  $\alpha_2$ ,  $\mu_1$ ,  $\mu_2$ , or  $\omega$  in [7]) to vary across plants, species, days, seasons, or sites may be appropriate. The above modifications to the root area model should be implemented with caution because the number of additional parameters that can be accommodated will depend on the quality and quantity of data and the sampling scheme.

Few studies have highlighted the potential utility of coupling information on soil water availability and plant and soil isotopes to infer water uptake patterns (Brunel *et al.*, 1995, Walker & Richardson, 1991), but none have explicitly linked the two sources of information. The RAPID algorithm does exactly this – it integrates stable isotopes and a biophysical model for root water uptake into a Bayesian inverse modeling framework. This novel and powerful new approach improves significantly upon the popular SLM models because it avoids the identifiability problem. Consequently, RAPID explicitly accounts for uncertainty in the estimates of water uptake, can reconstruct multiple (more than 3) water sources, and can provide estimates of the continuous water uptake profile provided the soil sampling resolution is fine enough. One of the most notable improvements over SLM models is that the RAPID algorithm provides information about the dynamics of the root system

itself – it reconstructs the profile of active root area for water uptake. The RAPID algorithm significantly advances the ability of plant, community, and ecosystem ecologists to unravel belowground processes.

**Acknowledgements.** The authors thank Roberto Fernández and Sarah Bauer for assistance in the field, and thanks to John Anderson (Jornada LTER) for logistic support in New Mexico. This work was supported by NASA Headquarters under the Earth System Science Fellowship (Grant # NGT5-30355), USDA (# 00-35101-9306), NSF (#DEB-02-12123), and is a contribution to the Jornada LTER (NSF Grant #DEB 94-11971). Soil and isotope analyses were also supported by Grants-in-Aid-of-Research (Sigma-Xi), Forrest Shreve Desert Research Award (Ecological Society of America), Grants-in-Aid-of-Research (Biology Dept., Duke), and Keever and Giles Awards for Research (Biology Dept., Duke).

## Appendix A: Prior Constraints

We evaluated the RAPID algorithm for two different priors. The first prior assumes that the continuous active root area profile,  $f_r(v)$ , is unimodal and can be depicted by a gamma distribution with shape parameter  $\alpha$  and mean  $\mu$ :

$$f_r(v | \alpha, \mu) \equiv \mathbf{Ga}(\alpha, \mu) \quad [9]$$

We choose lognormal priors for  $\alpha$  and  $\mu$  because both parameters are positive and because very small values of either are biologically unrealistic as they would yield unreasonably high proportions of root area near the soil surface. Thus, the prior is given by:

$$\begin{pmatrix} \ln(\alpha) \\ \ln(\mu) \end{pmatrix} \sim \text{No} \left( \begin{pmatrix} a \\ m \end{pmatrix}, C_{a,m} \right) \quad [10]$$

We also explored a 5-parameter gamma mixture model for estimating a potentially bimodal root area distribution:

$$f_r(v | \alpha_1, \alpha_2, \mu_1, \mu_2) \equiv \omega \cdot \mathbf{Ga}(\alpha_1, \mu_1) + (1 - \omega) \cdot \mathbf{Ga}(\alpha_2, \mu_2) \quad [11]$$

with shape parameters  $\alpha_1$  and  $\alpha_2$ , means  $\mu_1$  and  $\mu_2$ , and mixture weight  $\omega$ . For the same reasons outlined for the 2-parameter gamma model, we choose a multivariate normal prior for  $\ln(\alpha_1)$ ,  $\ln(\alpha_2)$ ,  $\ln(\mu_1)$ ,  $\ln(\mu_2)$  and  $\text{logit}(\omega)$  with covariance matrix  $B$ :

$$\begin{pmatrix} \ln(\alpha_1) \\ \ln(\alpha_2) \\ \ln(\mu_1) \\ \ln(\mu_2) \\ \text{logit}(\omega) \end{pmatrix} \sim \text{No} \left( \begin{pmatrix} a_1 \\ a_2 \\ m_1 \\ m_2 \\ w \end{pmatrix}, B \right) \quad [12]$$

Parameter values defining the prior distributions [10] and [8] were chosen to reflect current knowledge about *Larrea tridentata*'s root distribution and are given in Table A1.

**Table A1.** Constants used in the likelihood function [6] and prior distributions for the active root area profile parameters ([10], [8]).

Parameter(s)	Eqn.	Value(s)
$C_{D,O}$	[6]	$\begin{pmatrix} 3.29 & 0.62 \\ 0.62 & 0.29 \end{pmatrix}$
$\begin{pmatrix} a \\ m \end{pmatrix}$	[10]	$\begin{pmatrix} 2.0 \\ 3.5 \end{pmatrix}$
$C_{a,m}$	[10]	$\begin{pmatrix} 2.0 & 0.8 \\ 0.8 & 2.0 \end{pmatrix}$
$\begin{pmatrix} a_1 \\ a_2 \\ m_1 \\ m_2 \\ w \end{pmatrix}$	[8], [12]	$\begin{pmatrix} 1 \\ 3 \\ 3 \\ 4 \\ 0 \end{pmatrix}$
$B$	[8], [12]	$\begin{pmatrix} 1 & 0 & 0.3 & 0 & 0 \\ 0 & 1 & 0 & 0.3 & 0 \\ 0.3 & 0 & 0.5 & 0.4 & 0 \\ 0 & 0.3 & 0.4 & 0.8 & 0 \\ 0 & 0 & 0 & 0 & 2 \end{pmatrix}$

The likelihood covariance matrix  $C_{D,O}$  was estimated from the 25 stem samples described in the *Field Study* section and an additional 28 stem samples collected from eight near-by (within 30 m) *Larrea* shrubs during early July, 1998. The prior mean vectors were chosen to reflect current knowledge about *Larrea*'s root distribution (e.g., (Briones *et al.*, 1996, Freckman & Virginia, 1989, Kemp *et al.*, 1997, Moñtana *et al.*, 1995, Moorhead *et al.*, 1989)); the prior variances were inflated so that the priors' influence on the posterior estimates was minimal and thus the estimates are mostly driven by the data.

## Appendix B: Testing the RAPID Algorithm with Synthetic Data

**Synthetic Data Sets.** Before we applied the RAPID algorithm to the observed stem isotope data, we tested its ability to reconstruct "known" active root area profiles from synthetic data sets. We evaluated the ability of the algorithm to reconstruct twelve different "true" root area profiles, four of which we based on a gamma distribution (e.g. [9]) and the remaining eight we based on a mixture of gammas (e.g. [7], [11]). The twelve scenarios (Table B1) were chosen to represent a diversity of root area profiles that differed in the fraction of root area found in the top 0–2 cm, the fraction of root area beyond the maximum sampling depth (i.e., > 75 cm), the number of modes or peaks, and if bimodal, the degree of separation between and the relative importance of each mode. For each root area scenario, we simulated stem isotope data based on the root profiles, observed data for  $\Psi_r$ , observed soil isotope and water content ( $\delta D_{soil,i}$ ,  $\delta^{18}O_{soil,i}$ ,  $\theta_i$ ), and assumed that all soil samples were sandy-loam.

**Table B1.** Twelve active root area profiles used to evaluate the RAPID algorithm.

2-parameter gamma scenarios							
Scenario #	$\alpha$	$\mu$			%RA(>75 cm)*	%RA(0–2 cm)†	
2.1	1.0	30			8.20	6.40	
2.2	10.0	30			0.02	0.00	
2.3	3.0	60			27.70	0.02	
2.4	0.5	15			2.50	28.50	
5-parameter gamma scenarios							
Scenario #	$\alpha_1$	$\alpha_2$	$\mu_1$	$\mu_2$	$\omega$	%RA(>75 cm)*	%RA(0–2 cm)†
5.1	0.5	10	15	40	0.50	1.70	14.30
5.2	1.5	40	20	60	0.25	5.10	1.00
5.3	1.5	20	20	60	0.75	4.10	3.00
5.4	1.0	20	20	80	0.50	30.30	4.80
5.5	1.0	15	12	25	0.50	0.10	7.70
5.6	10.0	40	25	50	0.50	0.13	0.00
5.7	0.5	40	25	15	0.90	2.40	25.00
5.8	0.5	40	25	15	0.05	1.10	1.40

Scenarios 2.1–2.4 are based on a 2-parameter, unimodal gamma distribution (e.g., [9]) and Scenarios 5.1–5.8 are based on a 5-parameter, potential bimodal, mixture of gammas (e.g., [7], [11]).

\* The fraction of active root area occurring beyond 75 cm.

† The fraction of active root area in the 0–2 cm layer.

We then ran the RAPID algorithm for the 12 scenarios, each with 4 parallel MCMC chains of lengths  $J = 5,000$ . Posterior means and the central 95% CrIs were determined for the fractions of root area in each soil layer (i.e., each  $f_{r,i}$ ). The estimates were compared with the "true" fractions to determine under what scenarios the RAPID algorithm successfully reproduces the true root area profiles and to evaluate the performance of the 2- vs. 5-parameter gamma models for the root area distribution.

**Results: Reconstructing Known Root Area Profiles.** Because we started the MCMC chains near the posterior modes, all 96 chains (12 root profile scenarios  $\times$  2 root area models  $\times$  4 chains per scenario per model) noticeably converged after a burn-in (Brooks, 1998) of 1,000 iterations. Thus, posterior means and quantiles are based on the last 4,000 iterations. It is also important to note that in all cases (synthetic and observed data) the priors had little effect on the posterior estimates. For example, contour plots of the log likelihood and log posterior based on the 2-parameter model were nearly identical. The priors simply reduced

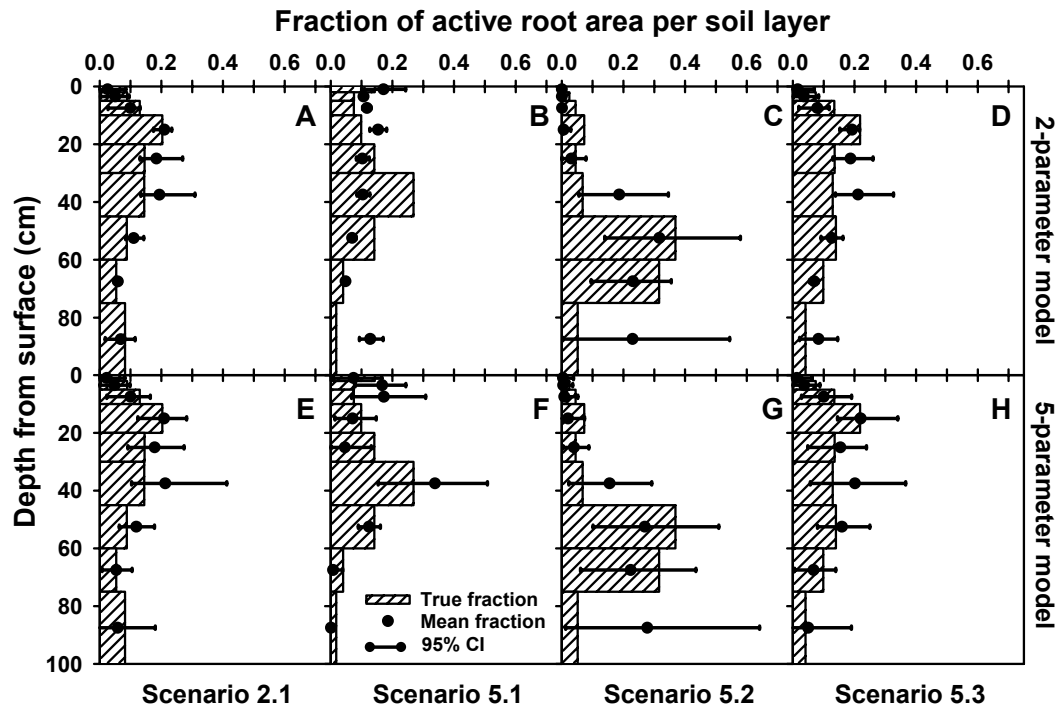


**Figure B1.** Posterior estimates of the active root area profiles based on fitting a 2-parameter (A–D) and 5-parameter (E–H) root area model. Results shown for synthetic data based on root area Scenarios 2.1 (A & E), 5.1 (B & F), 5.2 (C & G), and 5.3 (D & H). Posterior means and 95% CrI for the fraction of root area in soil layer are shown, along with the true fractions (bars).

**Table B2.** Goodness-of-fit statistics for the posterior root area fractions.

Scenario #	100xMSE*		100xMSE <sub>mean</sub> <sup>†</sup>		Max. 95% CrI width <sup>‡</sup>		True $f_{r,i}$ in CrI? <sup>§</sup>	
	2-parm	5-parm	2-parm	5-parm	2-parm	5-parm	2-parm	5-parm
2.1	0.167	0.304	0.095	0.129	0.176	0.309	Y	Y
2.2	0.201	0.420	0.008	0.164	0.358	0.416	Y	Y
2.3	0.480	0.841	0.096	0.239	0.551	0.669	N (1)	Y
2.4	0.101	0.095	0.085	0.042	0.129	0.154	N (6)	N (1)
5.1	0.608	0.636	0.583	0.432	0.143	0.354	N (8)	N (4)
5.2	1.198	1.514	0.701	0.908	0.541	0.629	N (4)	Y
5.3	0.269	0.316	0.194	0.110	0.188	0.310	N (4)	Y
5.4	0.266	0.459	0.162	0.041	0.245	0.504	N (4)	Y
5.5	0.642	0.169	0.615	0.054	0.096	0.268	N (6)	Y
5.6	0.635	0.470	0.458	0.198	0.351	0.392	N (3)	Y
5.7	0.042	0.150	0.026	0.021	0.129	0.274	N (3)	Y
5.8	0.215	0.358	0.061	0.145	0.364	0.364	N (1)	Y

Statistics and CrI values are for the posterior root area fractions predicted by the RAPID algorithm based on assuming a 2-parameter gamma model (2-parm; [9], [10]) and a 5-parameter gamma mixture model (5-parm; [7],[8]).

\*  $MSE = (N(J - j^* + 1)C)^{-1} \sum_{i=1}^N \sum_{j=j^*}^J \sum_{c=1}^C (f_{r,i}^{j,c} - \dot{f}_{r,i})^2$  where  $N = 9$  soil layers (the 9<sup>th</sup> layer represents 75+ cm);  $J - j^* + 1 = 4000$  iterations per chain ( $j^* - 1$  is the burn-in length); and  $C = 4$  parallel chains;  $f_{r,i}^{j,c}$  is the estimated root area fraction in soil layer  $i$ , iteration  $j$ , and chain  $c$ ;  $\dot{f}_{r,i}$  is the "true" root area fraction in layer  $i$ .

<sup>†</sup>  $MSE_{mean} = N^{-1} \sum_{i=1}^N \left[ \left( (C(J - j^* + 1))^{-1} \sum_{j=j^*}^J \sum_{c=1}^C f_{r,i}^{j,c} \right) - \dot{f}_{r,i} \right]^2$  describes the bias of the posterior mean fractions; i.e., index of how close the posterior mean value for  $f_{r,i}$  is to the true value.

<sup>‡</sup> 95% empirical posterior CrIs for the  $f_{r,i}$  values were determined for each soil layer and the maximum width (across 9 layers) is reported.

<sup>§</sup> If the true root area fractions of all nine soil layers are contained in their 95% CrIs, the a Y (yes). If at least one of the true fractions is not within it 95% CrI then an N (no) and the number of layers (out of 9) that fall outside of their respective 95% CrIs is given in parentheses.

the spread of the distributions so that the probability of extremely large or small values of  $\alpha$  and  $\mu$  was reduced.

The 2-parameter gamma root area model ([9], [10]) successfully reproduced the four 2-parameter, unimodal, true root area distributions (Scenarios 2.1–2.4; Table B1). The 2-parameter model was also equally successful at capturing the 5-parameter true root area profiles depicted by Scenarios 5.7 and 5.8; this is not surprising since these scenarios yielded profiles that were essentially 2-parameter, unimodal profiles because the mixture weights were either very close to one or zero. The shape of the posterior root area profiles for these six scenarios matched the true profiles remarkably well (e.g., see Fig. B1 A for Scenario 2.1).

For example, the posterior mean fractions were very close to the true fractions as indicated by small  $MSE_{\text{mean}}$  values (Table B2). The 2-parameter root area model was less successful at reconstructing the remaining true 5-parameter root area scenarios (Scenarios 5.1–5.6; Table B1), especially Scenarios 5.1 (e.g., Fig. B1 B) and 5.5, both of which exhibit pronounced bimodality (Table B2).

The 5-parameter model was equally successful at capturing the shape of the true 2-parameter root area profiles (Scenarios 2.1–2.4) (see Fig. B1 E for 2.1) and the two unimodal, 5-parameter root area scenarios (i.e., 5.7 and 5.8). In fact, the posterior means for the fraction of root area in each soil layer were indistinguishable from the posterior means based on the 2-parameter model. However, the posterior mean fractions for Scenarios 5.1–5.6 were noticeably improved by employing the 5-parameter model (see Fig. B1 F–H). With the exception of a few soil layers in Scenarios 2.4 and 5.1, all 95% posterior CrIs for the root area fractions based on the 5-parameter model contained the true fractions. Thus, the 5-parameter model was able to reconstruct a variety a root area profiles that varied in degree of bimodality and general shape.

It is worth comparing the performances of the 2- and 5-parameter models. For nearly all of the scenarios, the 2-parameter model resulted in smaller MSEs and narrower CrIs (Table B2, Fig. B1). However, while narrower CrIs are typically preferred because they might indicate greater accuracy or less uncertainty in the estimates, in this case the smaller widths resulted in CrIs that often did not contain the true fractions. Apparently the 5-parameter model is more realistic in its ability to represent uncertainty in the root area fractions as its wider CrIs frequently contain the true fractions. The posterior mean fractions based on the 5-parameter model are also typically less biased for the true fractions than the 2-parameter posterior means, as depicted by the smaller  $MSE_{\text{mean}}$  values in Table B2. Finally, discrepancies between the posterior estimates based on the 5-parameter model and the true fractions could not be attributed to root area characteristics such as degree of bimodality, mixing weight, or the fraction of roots in the top 2 cm or beyond 75 cm. Conversely, differences between estimates based on the 2-parameter model and the true fractions were clearly greater when the true profiles exhibited bimodality.

Overall, the 5-parameter model was superior to the 2-parameter model at reconstructing the known root area profiles. This was expected because the additional three

parameters provided greater flexibility and yielded posterior distributions that better reflect uncertainty. It is recommended that the 5-parameter be employed over the 2-parameter model because in reality, we do not know if the root profile is bimodal or not. The 5-parameter model is able to reconstruct both unimodal and bimodal profiles, while the 2-parameter model is restricted to unimodal ones. In general, when employing the 5-parameter model, the biophysical model within the Bayesian approach successfully reconstructed a diversity of root area profiles while explicitly accounting for uncertainty in the estimates.

## Appendix C: Details on the MCMC Routine

We constructed contour plots of the posterior density to locate the range of values of  $\alpha$  and  $\mu$  (or  $\alpha_1, \alpha_2, \mu_1, \mu_2$ , and  $\omega$ ) that yield the highest posterior probabilities (i.e., we located the posterior mode) (Cowles & Carlin, 1996). We generated independent starting values of  $\ln(\alpha)$  and  $\ln(\mu)$  (or  $\ln(\alpha_1), \ln(\alpha_2), \ln(\mu_1), \ln(\mu_2)$ , and  $\text{logit}(\omega)$ ) from a uniform distribution centered at the mode (Step 1 in the MCMC routine). We used a Gaussian random walk (on the natural log scale) for the transition density  $Q(\alpha^*, \mu^* | \alpha^{(j-1)}, \mu^{(j-1)})$ :

$$\begin{pmatrix} \ln(\alpha^*) \\ \ln(\mu^*) \end{pmatrix} \sim \text{No} \left( \begin{pmatrix} \ln(\alpha^{(j-1)}) \\ \ln(\mu^{(j-1)}) \end{pmatrix}, \begin{pmatrix} \tau_\alpha^2 & 0 \\ 0 & \tau_\mu^2 \end{pmatrix} \right) \quad [13]$$

A similar Gaussian random walk was employed for the 5-parameter model to generate independent values for  $\ln(\alpha_1), \ln(\alpha_2), \ln(\mu_1), \ln(\mu_2)$  and  $\text{logit}(\omega)$ . While the parameters were generated from  $Q(\cdot | \cdot)$  in a single step, acceptance of parameters was determined individually (e.g., systematic sweep, Brooks, 1998) and their step sizes were chosen so that proposal values were accepted approximately 30 to 60% of the time (Roberts *et al.*, 1997, Roberts & Rosenthal, 2001). Because we reparameterized the root model with  $\ln(\alpha_1), \ln(\alpha_2), \ln(\mu_1), \ln(\mu_2)$  and  $\text{logit}(\omega)$ ,  $Q(\cdot | \cdot)$  is symmetric,  $Q(y|z) = Q(z|y)$ , and the acceptance ratio reduces to a ratio of the posteriors (Brooks, 1998, Chib & Greenberg, 1995, Metropolis *et al.*, 1953):

$$\lambda = \frac{P(\alpha^*, \mu^* | \text{Data})}{P(\alpha^{(j-1)}, \mu^{(j-1)} | \text{Data})} \quad [14]$$

## Appendix D: Details on field Methods and Stable Isotope Analyses

**Stem water.** During the morning on each sampling date, five woody stem samples were collected from each shrub and immediately placed in Opticlear vials (borosilicated glass with polyethylene stopper), double sealed with parafilm, kept in an ice chest with solid CO<sub>2</sub> for the day, and thereafter stored at approximately –20°C until the water was extracted for δD and δ<sup>18</sup>O analyses.

**Soil water and texture.** The soil subsamples that we collected for stable isotope analyses were immediately placed in Saranex leak-proof re-closable bags and stored with the stem samples. Soil texture (i.e., particle size; % sand, silt and clay) was determined for each soil sample; analyses were completed by Brookside Laboratories, New Knoxville, OH. For those cores that did not extend to 75 cm, soil water content and isotopic composition for missing sections were estimated with the average of the other sections at the same depth within the core or with the value of the previous depth if all three cores within a day were missing the same section(s). Soil texture data were analyzed in an ANOVA with date and depth (midpoint of each soil layer) as fixed factors and we used the results to estimate missing texture data.

**Laboratory analyses.** Water was extracted from the stem and soil samples during March 2002 at the Center for Stable Isotope Biogeochemistry (CSIB) on the University of California, Berkeley campus. Extractions were done via cryogenic distillation (Ehleringer & Osmond, 1989) and the water was immediately placed in a plastic vial and parafilm over the cap for a tight seal. Activated carbon was added to the stem water samples to remove resins. Water samples were analyzed for natural abundance of D and <sup>18</sup>O during April and May 2002 on a Finnigan-MAT Delta Plus XL mass spectrometer. Isotopic signatures, δD and δ<sup>18</sup>O (per mil, ‰), were calculated relative to Standard Mean Ocean Water (SMOW) as:

$$\delta X = 1000 \cdot \left( \frac{R_{sample}}{R_{SMOW}} - 1 \right) \quad [15]$$

where X = D or <sup>18</sup>O and  $R_{sample}$  and  $R_{SMOW}$  are the isotopic abundance ratios of the sample and standard, respectively (i.e., D/H or <sup>18</sup>O/<sup>16</sup>O).

## Appendix E: Sensitivity Analysis

**Water Uptake and Plant Root Parameters.** Root radius,  $r_r$ , and total root area,  $RA_{tot}$ , are required for the root water uptake model [4]. We set  $r_r$  equal to 0.1 mm (e.g., Caldwell & Richards, 1986) and fixed  $RA_{tot}$  at  $1.0 \text{ m}^2$ . We conducted a sensitivity analysis where we varied  $r_r$  and  $RA_{tot}$  up and down by several orders of magnitude and ran the MCMC algorithm for each value. Changing  $r_r$  and  $RA_{tot}$  did not affect the posterior distributions of  $\alpha$  and  $\mu$  (or  $\alpha_1$ ,  $\alpha_2$ ,  $\mu_1$ ,  $\mu_2$ , and  $\omega$ ) and  $f_{r,i}$ .

## Literature Cited

- Allison, G.B. & Hughes, M.W. (1983). The use of natural tracers as indicators of soil-water movement in a temperate semi-arid region. *Journal of Hydrology*, **60**: 157-173.
- Barnes, C.J. & Allison, G.B. (1988). Tracing of water movement in the unsaturated zone using stable isotopes of hydrogen and oxygen. *Journal of Hydrology*, **100**: 143-176.
- BassiriRad, H., Tremmel, D.C., Virginia, R.A., Reynolds, J.F., de Soyza, A.G. & Brunell, M.H. (1999). Short-term patterns in water and nitrogen acquisition by two desert shrubs following a simulated summer rain. *Plant Ecology*, **145**: 27-36.
- Briones, O., Montaña, C. & Ezcurra, E. (1998). Competition intensity as a function of resource availability in a semiarid ecosystem. *Oecologia*, **116**: 365-372.
- Briones, O., Moñtana, C. & Ezcurra, E. (1996). Competition between three Chihuahuan desert species: evidence from plant size-distance relations and root distribution. *Journal of Vegetation Science*, **7**: 453-460.
- Brooks, S.P. (1998). Markov chain Monte Carlo method and its application. *The Statistician*, **47**: 69-100.
- Brunel, J.-P., Walker, G.R. & Kennett-smith, A.K. (1995). Field validation of isotopic procedures for determining sources of water used by plants in a semi-arid environment. *Journal of Hydrology*, **167**: 351-368.
- Cable, D.R. (1980). Seasonal patterns of soil water recharge and extraction on semidesert ranges. *Journal of Range Management*, **33**: 9-15.
- Caldwell, M.M. & Richards, J.H. (1986) Competing root systems: morphology and models of absorption. In: *On the Ecology of Plant Form and Function* (ed T.J. Givnish), pp. 251-273. Cambridge University Press, Cambridge.
- Campbell, G.S. (1991) Simulation of water uptake by plant roots. In: *Modeling Plant and Soil Systems* (eds J. Hanks & J.T. Ritchie), pp. 273-285. American Society of Agronomy, Inc., Madison, WI.
- Chib, S. & Greenberg, E. (1995). Understanding the Metropolis-Hasting algorithm. *The American Statistician*, **49**: 327-335.
- Conley, W., Conley, M.R. & Karl, T.R. (1992). A computational study of episodic events and historical context in long-term ecological processes: climate and grazing in the northern Chihuahuan Desert. *Coenoses*, **7**: 55-60.
- Cowles, M.K. & Carlin, B.P. (1996). Markov chain Monte Carlo convergence diagnostics: a comparative review. *Journal of the American Statistical Association*, **91**: 883-904.
- Cramer, V.A., Thorburn, P.J. & Fraser, G.W. (1999). Transpiration and groundwater uptake from farm forest plots of *Casuarina glauca* and *Eucalyptus camaldulensis* in saline areas of southeast Queensland, Australia. *Agricultural Water Management*, **39**: 187-204.
- Dansgaard, W. (1964). Stable isotopes in precipitation. *Tellus*, **16**: 436-468.

- Dawson, T.E. & Ehleringer, J.R. (1998) Plants, isotopes and water use: A catchment-scale perspective. In: *Isotope Tracers in Catchment Hydrology* (eds C. Kendall & J.J. McDonnell), pp. 165-202. **Elsevier Science**, Amsterdam.
- Ehleringer, J.R. & Dawson, T.E. (1992). Water uptake by plants: perspectives from stable isotope composition. *Plant Cell and Environment*, **15**: 1073-1082.
- Ehleringer, J.R. & Osmond, C.B. (1989) Stable isotopes. In: *Plant Physiological Ecology: Field Methods and Instrumentation* (eds R.W. Pearcy, J. Ehleringer, H.A. Mooney, & P.W. Rundel), pp. 281-300. Chapman & Hall, London.
- Ehleringer, J.R., Phillips, S.L., Schuster, W.S.F. & Sandquist, D.R. (1991). Differential utilization of summer rains by desert plants. *Oecologia*, **88**: 430-434.
- Ewe, S.M.L., Sternberg, L.D.L. & Busch, D.E. (1999). Water-use patterns of woody species in pineland and hammock communities of South Florida. *Forest Ecology and Management*, **118**: 139-148.
- Feild, T.S. & Dawson, T.E. (1998). Water sources used by *Didymopanax pittieri* at different life stages in a tropical cloud forest. *Ecology*, **79**: 1448-1452.
- Fernandez, O.A. & Caldwell, M.M. (1975). Phenology and dynamics of root growth of three cool semi-desert shrubs under field conditions. *Journal of Ecology*, **63**: 703-714.
- Freckman, D.W. & Virginia, R.A. (1989). Plant-feeding nematodes in deep-rooting desert ecosystems. *Ecology*, **70**: 1665-1678.
- Gelman, A. (1996) Inference and monitoring convergence. In: *Markov Chain Monte Carlo in Practice* (eds W.R. Gilks, S. Richardson, & D.J. Spiegelhalter), pp. 131-143. Chapman & Hall, Boca Raton.
- Hacke, U.G., Sperry, J.S., Ewers, B.E., Ellsworth, D.S., Schäfer, K.V.R. & Oren, R. (2000). Influence of soil porosity on water use in *Pinus taeda*. *Oecologia*, **124**: 495-505.
- Hastings, W.K. (1970). Monte Carlo sampling methods using Markov chains and their applications. *Biometrika*, **57**: 97-109.
- Huang, B.R. & Fu, J.M. (2000). Photosynthesis, respiration, and carbon allocation of two cool-season perennial grasses in response to surface soil drying. *Plant and Soil*, **227**: 17-26.
- Jobbágy, E.G. & Jackson, R.B. (2001). The distribution of soil nutrients with depth: global patterns and the imprint of plants. *Biogeochemistry*, **53**: 51-77.
- Kemp, P.R., Reynolds, J.F., Pachepsky, Y. & Chen, J.-L. (1997). A comparative modeling study of soil water dynamics in a desert ecosystem. *Water Resources Research*, **33**: 73-90.
- McCully, M.E. (1999). Root xylem embolisms and refilling. Relation to water potentials of soil, roots, and leaves, and osmotic potentials of root xylem sap. *Plant Physiology*, **119**: 1001-1008.
- Metropolis, N., Rosenbluth, A.W., Teller, M.N. & Teller, E. (1953). Equations of state calculations by fast computing machines. *Journal of Chemical Physics*, **21**: 1087-1092.

- Midwood, A.J., Boutton, T.W., Archer, S.R. & Watts, S.E. (1998). Water use by woody plants on contrasting soils in a savanna parkland: assessment with  $\delta\text{H}^2$  and  $\delta^{18}\text{O}$ . *Plant and Soil*, **205**: 13-24.
- Moñtana, C., Cavagnaro, B. & Briones, O. (1995). Soil water use by co-existing shrubs and grasses in the Southern Chihuahuan Desert, Mexico. *Journal of Arid Environments*, **31**: 1-13.
- Moorhead, D.L., Reynolds, J.F. & Fonteyn, P.J. (1989). Patterns of stratified soil water loss in a Chihuahuan Desert community. *Soil Science*, **148**: 244-249.
- Neath, A.A. & Samaniego, F.J. (1997). On the efficacy of Bayesian inference for nonidentifiable models. *American Statistician*, **51**: 225-232.
- Phillips, D.L. & Gregg, J.W. (2001a). Uncertainty in source partitioning using stable isotopes. *Oecologia*, **127**: 171-179.
- Phillips, D.L. & Gregg, J.W. (2001b). Uncertainty in source partitioning using stable isotopes: erratum. *Oecologia*, **128**: 304.
- Plamboeck, A.H., Grip, H. & Nygren, U. (1999). A hydrological tracer study of water uptake depth in a Scots pine forest under two different water regimes. *Oecologia*, **119**: 452-460.
- Pregitzer, K.S., DeForest, J.L., Burton, A.J., Allen, M.F., Ruess, R.W. & Hendrick, R.L. (2002). Fine root architecture of nine North American trees. *Ecological Monographs*, **72**: 293-309.
- Retzlaff, W.A., Blaisdell, G.K. & Topa, M.A. (2001). Seasonal changes in water source of four families of loblolly pine (*Pinus taeda* L.). *Trees-Structure and Function*, **15**: 154-162.
- Reynolds, J.F., Virginia, R.A., Kemp, P.R., de Soyza, A.G. & Tremmel, D.C. (1999). Impact of drought on desert shrubs: effects of seasonality and degree of resource island development. *Ecological Monographs*, **69**: 69-106.
- Robert, C.P. & Casella, G. (1999) *Monte Carlo Statistical Methods*. Springer-Verlag, New York.
- Roberts, G.O., Gelman, A. & Gilks, W.R. (1997). Weak convergence and optimal scaling of random walk Metropolis algorithms. *Annals of Applied Probability*, **7**: 110-120.
- Roberts, G.O. & Rosenthal, J.S. (2001). Optimal scaling for various Metropolis-Hastings algorithms. *Statistical Science*, **16**: 351-367.
- Sala, O.E., Lauenroth, W.K. & Parton, W.J. (1992). Long-term soil water dynamics in the shortgrass steppe. *Ecology*, **73**: 1175-1181.
- Schenk, H.J. & Jackson, R.B. (2002). The global biogeography of roots. *Ecological Monographs*, **72**: 311-328.
- Schlesinger, W.H., Fonteyn, P.J. & Marion, G.M. (1987). Soil moisture content and plant transpiration in the Chihuahuan Desert of New Mexico. *Journal of Arid Environments*, **12**: 119-126.

- Schwinnig, S., Davis, K., Richardson, L. & Ehleringer, J.R. (2002). Deuterium enriched irrigation indicates different forms of rain use in shrub/grass species of the Colorado Plateau. *Oecologia*, **130**: 345-355.
- Snyder, K.A. & Williams, D.G. (2000). Water sources used by riparian trees varies among stream types on the San Pedro River, Arizona. *Agricultural and Forest Meteorology*, **105**: 227-240.
- Solbrig, O.T. (1977) The adaptive strategies of *Larrea*. In: *Creosote Bush: Biology and Chemistry of Larrea in New World Deserts, US/IBP Synthesis Series 6* (eds T.J. Mabry, J.H. Hunziker, & D.R. Difeo, Jr.), pp. 1-9. Halsted Press, New York.
- Sperry, J.S., Adler, F.R., Campbell, G.S. & Comstock, J.P. (1998). Limitation of plant water use by rhizosphere and xylem conductance: results from a model. *Plant, Cell and Environment*, **21**: 347-359.
- Thorburn, P.J. & Ehleringer, J.R. (1995). Root water uptake of field-growing plants indicated by measurements of natural-abundance deuterium. *Plant and Soil*, **177**: 225-233.
- Thorburn, P.J. & Walker, G.R. (1993) The source of water transpired by *Eucalyptus camaldulensis*: Soil, groundwater, or streams? In: *Stable Isotopes and Plant Carbon-Water Relations* (eds J.R. Ehleringer, A.E. Hall, & G.D. Farquhar), pp. 511-527. Academic Press, San Diego.
- Thorburn, P.J., Walker, G.R. & Brunel, J.-P. (1993). Extraction of water from *Eucalyptus* trees for analysis of deuterium and oxygen-18: laboratory and field techniques. *Plant Cell and Environment*, **16**: 269-277.
- Vandenbeldt, R.J. (1991). Rooting systems of western and southern African *Faidherbia albida* (Del.) A. Chev (syn. *Acacia albida* Del.) – a comparative analysis with biogeographic implications. *Agroforestry Systems*, **14**: 233-244.
- Walker, C.D. & Richardson, S.B. (1991). The use of stable isotopes of water in characterising the source of water in vegetation. *Chemical Geology Isotope Geoscience Section*, **94**: 145-158.
- Wan, C., Sosebee, R.E. & McMichael, B.L. (1994). Hydraulic properties of shallow vs. deep lateral roots in a semiarid shrub, *Gutierrezia sarothrae*. *American Midland Naturalist*, **131**: 120-127.
- Weaver, T. (1982). Distribution of root biomass in well-drained surface soils. *American Midland Naturalist*, **107**: 393-395.
- White, J.W.C., Cook, E.R., Lawrence, J.R. & Broecker, W.S. (1985). The D/H ratios of sap in trees: implications for water sources and tree ring D/H ratios. *Geochimica et Cosmochimica Acta*, **49**: 237-246.